Acta Oceanol. Sin., 2024, Vol. 43, No. 4, P. 136–150
https://doi.org/10.1007/s13131-024-2332-x
http://www.aosocean.com
E-mail: ocean2@hyxb.org.cn

Astronomical influence of the development of Paleogene thin coal seam groups in offshore Lacustrine basins: A case study of the Zhu Ⅰ Depression's Enping Formation located in the northern South China Sea

Yan Liu[1], Shengbing Huang[2], Dongdong Wang[1, 3*], Nan Li[2], Yuting Yin[1], Ying Chen[2], Zengxue Li[1]

[1] College of Earth Science and Engineering, Shandong University of Science and Technology, Qingdao 266590, China

[2] CNOOC Research Institute Co., Ltd., Beijing 100028, China

[3] School of Geography, Earth and Environmental Sciences, University of Birmingham, Birmingham B15 2TT, UK

Received 18 April 2023; accepted 6 September 2023

Abstract

The development of the Paleogene coal seams in China's offshore basin areas generally had the characteristics of coal measures with large thicknesses, large numbers of coal seams, thin single coal seams, poor stability, scattered vertical distribution, and a wide distribution range. This study selected the Enping Formation of the Zhu Ⅰ Depression in the northern section of the South China Sea as an example to determine the macro-control factors of the development of the Paleogene coal seam groups. An analysis was carried out on the influencing effects and patterns of the astronomical cycles related to the development of the thin coal seam groups in the region. A floating astronomical time scale of the Enping Formation was established, and the sedimentary time limit of the Enping Formation was determined to be approximately 6.15 Ma±. In addition, the cyclostratigraphy analysis results of the natural gamma-ray data of Well XJ in the Enping Formation of the Xijiang Sag revealed that the development of the thin coal seams had probably been affected by short eccentricity and precession factors. The formation process of coal seams was determined to have been affected by high seasonal contrast, precipitation, and insolation. During the periods with high values of short eccentricity, the seasonal contrasts tended to be high. During those periods, fluctuations in the precession controls resulted in periodic volume changes in precipitation and insolation of the region, resulting in the development of thin coal seams. It was also found that the periods with low precession were the most conducive to coal seam development. On that basis, combined with such factors as sedimentary environmental conditions conducive to the development of thin coal seam groups, this study established a theoretical model of the comprehensive influences of short eccentricity and precession on the development and distribution of Paleogene thin coal seam groups in offshore lacustrine basins. The patterns of the Paleogene astronomical periods and paleoclimate evolution, along with the control factors which impacted the development of thin coal seam groups in offshore lacustrine basins, were revealed.

Key words: Paleogene, Pearl (Zhujiang) River Mouth Basin, coal seam development, astronomical cycles

Citation: Liu Yan, Huang Shengbing, Wang Dongdong, Li Nan, Yin Yuting, Chen Ying, Li Zengxue. 2024. Astronomical influence of the development of Paleogene thin coal seam groups in offshore Lacustrine basins: A case study of the Zhu Ⅰ Depression's Enping Formation located in the northern South China Sea. Acta Oceanologica Sinica, 43(4): 136–150, doi: 10.1007/s13131-024-2332-x

1 Introduction

Coal formation processes were very common in the Cenozoic coal-forming periods of offshore basins in China (Zhang et al., 2007, 2010, 2014a, 2016b), and were important parts of the circum-Pacific coal-accumulating belt. However, the coal formation processes were restricted by such geological conditions as palaeoclimate, palaeostructure, and palaeogeography (Li et al., 2012b). In recent years, some achievements have been made in the study of Cenozoic coal formation and coal-measure source rock in China sea area (Li et al., 2022; Zhang et al., 2020c; Wang et al., 2011, 2021; Shao et al., 2021). It has been found that the development characteristics of the Cenozoic coal measures in China's offshore basins generally include coal measures with large thicknesses, large numbers of coal seams, thin single coal seams, poor stability, scattered vertical distribution, and a wide distribution range (Zhang et al., 2022; Li et al., 2012b). However, the controlling factors and the formation mechanisms remain unclear for the general characteristics of the development of the Cenozoic coal seams in the offshore areas. It has been speculated that the coal-seam development may have been controlled

Foundation item: The Scientific Research Project under contract No. CCL2021RCPS172KQN; the Formation Mechanism and Distribution Prediction of Cenozoic Marine Source rocks in Qiongdongnan and Pearl River Mouth Basin under contract No. 2021-KT-YXKY-01; the Resource Potential, Accumulation Mechanism and Breakthrough Direction of Potential Oil-rich Sags in Offshore Basins of China under contract No. 2021-KT-YXKY-03; the National Natural Science Foundation of China (NSFC)under contract No. 42372132; the Open Foundation of Hebei Provincial Key Laboratory of Resource Survey and Research;the National Natural Science Foundation of China (NSFC) under contract Nos 42072188, 42272205.
*Corresponding author, E-mail: wdd02_1@163.com

by macro factors beyond the scope of the basins.

Cyclostratigraphy can be used to speculate changes in astronomical cycles by analyzing a series of geochemical or physical indicators and then constructing an astronomical time scale (ATS) with high resolution to statistically analyze orbital cycles. It has successfully been applied to Cenozoic, Mesozoic, and Paleozoic strata (Hinnov, 2013; Abels et al., 2010).

Previous research results have revealed that astronomical periodic forces affected surface environments, biota, and climate at a macro level (Tyszka, 2009; Husinec and Read, 2018). Many previous research studies have shown the existence of climatic orbital forces in various Cenozoic coal-forming environments, and the relationships between coal seams and different astronomical parameters have been determined (Noorbergen et al., 2018; Valero et al., 2016). Therefore, based on the previous research findings, it has been speculated that the development of Cenozoic coal seams in China sea area may have been macro-controlled by astronomical cycles. At present, relevant studies have indicated possible relationships between the development of thin coal seams in China sea area and the astronomical cycles of the Cenozoic (Zhang et al., 2016a; Shen et al., 2016; Zhao et al., 2022). However, the possible influencing effects of astronomical cycles remain vague, and the causes of the formation of thin coal seams are still controversial. Further research is needed to explore the genetic relationships and patterns which impacted the development of the thin coal seams in China's offshore basins.

In this study, the coal measures of the Paleogene Enping Formation in the northern section of the South China Sea (SCS) were taken as examples, and the correlations between the astronomical cycles and coal seam development were examined using the theories and methods of cyclostratigraphy and coal geology. A comparative analysis of the relationships between the coal seams of the Enping Formation and the orbital cycles was completed, and the controlling effects and patterns of the astronomical cycles related to the formation of the Paleogene thin coal seams were discussed. The results obtained in this study further enrich the basic geological theory of coal geology and support a better understanding of the influence of the Paleogene climate on the sedimentary environments of offshore basins.

2 Geological settings

2.1 *Location*

The Pearl (Zhujiang) River Mouth Basin (PRMB) is a Cenozoic basin developed in the northern SCS (Zhang, 2010; Zhang et al., 2013). It is located at the intersection of the Pacific Plate, Indian-Australian Plate, and the Eurasian Plate (Zhang et al., 2015a, 2015b, 2018). The PRMB has a complex geodynamic background and evolutionary structure, as detailed in Fig. 1. The basin has a tectonic framework characterized by NE-trending sags and uplifts. As shown in Fig. 1, from north to south, it consists of northern uplifts; northern sags (including the Zhu Ⅰ Depression and Zhu Ⅲ Depression); central uplifts (including the Shenhu Uplift, Panyu Low Uplift, and Dongsha Uplift); southern sags; and southern uplifts. The Zhu Ⅰ Depression is a Cenozoic depression located near land in southern China that is distributed in the NE direction on the plain. The depression includes the Enping Sag, Xijiang Sag, and Huizhou Sag, as well as other sags and secondary sags (Zhang et al., 2013). Furthermore, the PRMB was situated at a low latitude (~ 20°N) during the early Oligocene period (Boucot et al., 2013).

2.2 *Structural characteristics and evolution*

The PRMB is mainly composed of three groups of faults: NNE-NE-trending right-lateral tensile-torsional faults; NWW-NW-trending left-lateral strike-slip faults; and near EW-NEE-trending faults dominated by listric normal faults (Cheng et al., 2012; Li et al., 2012a; Wang et al., 2017) (Fig. 1a). During the Cenozoic, the PRMB experienced six major tectonic events, in which the first and second episodes of the Zhuqiong Movement played important roles in the episodic rifting of the Paleogene basins. In the early stage of the deposition of the Wenchang

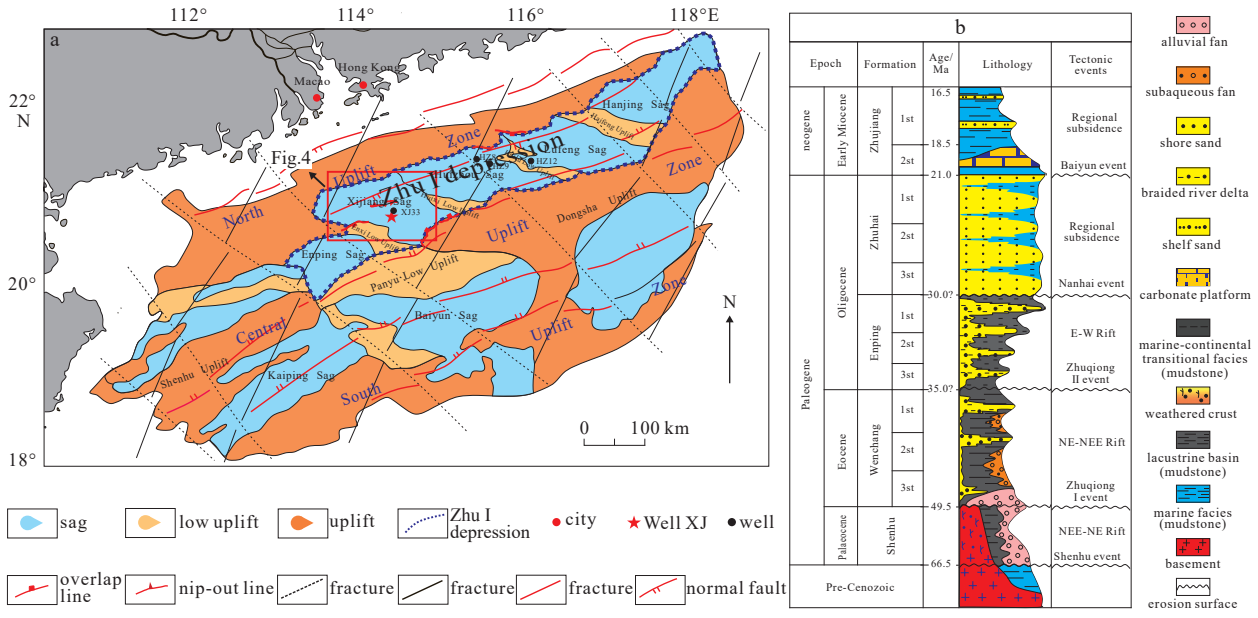

Fig. 1. Geographical location, tectonic units and comprehensive column of the study area. a. The tectonic units of PRMB and Zhu Ⅰ Depression are located in PRMB, showing the location of wells (refer to Wang et al., 2017, modified). b. Comprehensive histogram of PRMB tectonic evolution (Jiang et al., 2009; Zhang et al., 2020a; Wei et al., 2020).

Formation, the basin was generally uplifted and denuded, with volcanic magma and faulted tectonic activities occurring during the period. Two fault depression zones were formed in the north and south of the basin, spreading in a NE-NEE direction (Guo, 2015). The second episode occurred during a transition period between the Wenchang Formation and the Enping Formation. The basin was strongly uplifted and denuded at that time, and a large-scale EW-trending fault system was formed in the Zhu Ⅰ Depression. The lacustrine basin area had increased during the second episode compared to the first episode. However, the lake became shallower during that period (Peng et al., 2022) (Fig. 1b). Furthermore, in the sedimentary period of the Enping Formation in the Zhu Ⅰ Depression, the thicknesses of the roots of the fault footwalls of each secondary depression were obviously larger than those of the fault depression centers. The basic structural units were "half graben" and "graben" structures, and the geometric shapes of the different depressions were basically the same.

2.3 *Strata*

The Wenchang Formation, Enping Formation, Zhuhai Formation, and Zhujiang Formation were successively deposited in the PRMB following several tectonic events during the Cenozoic. The Wenchang Formation was deposited in the Middle Eocene and was formed after the Zhuqiong episode of the rifting period. The lithology is mainly mudstone, thin sandstone, and siltstone. Occasional coal seams and igneous rock can be seen in some areas. The Enping Formation is the overlying strata of the Wenchang Formation. It was formed after the second episode of the Zhuqiong Movement of the rifting period and displays unconformity with the overlying and underlying strata. The lithology of the area is mainly sandstone and dark gray mudstone mixed with carbonaceous mudstone and coal measure strata (Li, 2015). The coal seams in the Enping Formation are generally thin, with a relatively large number of layers, even dozens of layers in some locations. In the study area, the coal seams which have developed in depressions have obvious differences in characteristics (such as number and thickness) due to various geological factors (Yin, 2022). The Zhuhai Formation was deposited during the Oligocene and formed during a period of fault-depression transformation. The lithology is mainly light gray medium-thick medium sandstone, along with medium-thin mudstone and occasional thin coal seams. The Zhujiang Formation was deposited during the Miocene depression stage. Its lithology is mainly gray calcareous mudstone and limestone, with occasional traces of thin siltstone (Guo, 2015).

2.4 *Determination of the geological age*

The age of the Enping Group is still controversial due to the lack of a confirmed absolute age. Li and Ma (1992) determined that planktonic foraminifers and calcareous nannofossils exist in the Enping Formation through a comparison of the characteristics of the sporopollen assemblages and classified the Enping Formation as Oligocene. Lei (1993) used a K-Ar dating method to determine that the absolute age of the tuff in the Enping Formation was 35.5 Ma ± 2.8 Ma, and then divided the Enping Formation into Eocene strata. In another related study, based on the analysis results of drilling biostratigraphy data, Huang and Zhong (1998), Huang (1999) determined that the age of the Wenchang Formation was Middle-Late Eocene, in accordance with the calcareous nannofossil zones, sporopollen fossil assemblages, and planktonic foraminifera of the formation. Wu et al. (2003) examined the pollen records in the shallow sea areas of the northern SCS and determined that the boundary ages of the Enping and Zhuhai Formations in the PRMB region were approximately 32.0 Ma. Ren and Lei (2011) identified the conversion interface T70 between the Enping Formation and the Zhuhai Formation and estimated the age of the interface to be between 32.0 Ma and 30.0 Ma.

According to the results of a zircon study conducted by Shao et al. (2017), the Middle-Late Eocene sediment roughly corresponded to the lacustrine-neritic facies of the Wenchang and Enping Formations in the PRMB. In addition, based on the analysis results of palynological assemblages and calcareous nannofossils, Zhang et al. (2020a) determined that the bottom interface of the Enping Formation was formed at approximately 39.0 Ma and the top interface was formed between 33.0 Ma and 34.0 Ma. Tang et al. (2020) measured the age range of the sandstone strata at 2 870 m in Well LF13-2 of the Enping Formation using a zircon U-Pb dating analysis method and determined the range to be between 32.0 Ma and 38.0 Ma. The age range of the sandstone strata at 3 803 m in Well PY5-2 of the Wenchang Formation was estimated to be between 38.0 Ma and 49.0 Ma. Zhou et al. (2020) used detrital a zircon U-Pb dating analysis method to determine that the youngest age of the second member of the Wenshan Formation as approximately 39.1 Ma, and the youngest age of the fifth member of the Wenshan Formation as approximately 43.0 Ma. Wei et al. (2020) set the boundary between the Wenchang Formation and the Enping Formation as the Eocene-Oligocene boundary and adopted a cyclostratigraphy analysis method to obtain the age of the Enping Formation as between 33.9 Ma and 29.0 Ma. The central Italian marine system is marked by the extinction of planktonic foraminifera, and the Eocene-Oligocene boundary age has been defined as 33.9 Ma ± 0.1 Ma (Boulila et al., 2011; Galeotti et al., 2016). In addition, Xia (2022) has determined the age of the boundary between the Wenchang Formation and the Enping Formation to be approximately 33.8 Ma through cyclostratigraphy analysis processes. Peng et al. (2023a) reconstructed the climatic evolution during the sedimentary period and defined the Enping Formation as late Eocene based on the results of palynology and elemental analyses of the lacustrine sediment.

In summary, previous research results have shown that the Wenchang Formation in the PRMB belongs to the Middle-Late Eocene, with the general ages of the top strata being approximately 39.0 Ma, 33.9 Ma, 40.0 Ma, and so on. Moreover, previous research findings suggest that the expressions of the orbital periods in low latitudes may have been dominated by eccentricity in the Eocene, while eccentricity, obliquity, and precession were dominant in the Oligocene (Xu et al., 2023; Li et al., 2016b). As detailed in Fig. 2, by combining the previous research findings and the expressions of precession during the period, this study defined the Enping Formation as early Oligocene strata and estimated the bottom age as approximately 33.9 Ma.

2.5 *Sedimentary environments*

The first member of the Wenchang Formation under the lower part of the Enping Formation in the Zhu Ⅰ Depression had only been deposited in a small area, with discontinuity in a larger area (Wu et al., 2021). This study found that the Enping Formation was mainly composed of thick middle sandstone interspersed with thin mudstone, and both the overlying and underlying strata were in unconformable contact. In the Enping Formation, braided river delta (Figs 3a and b), lacustrine (Fig. 3c), and fan delta facies had mainly developed (Yin, 2022). The coal seams of the Enping Formation are relatively well developed. The char-

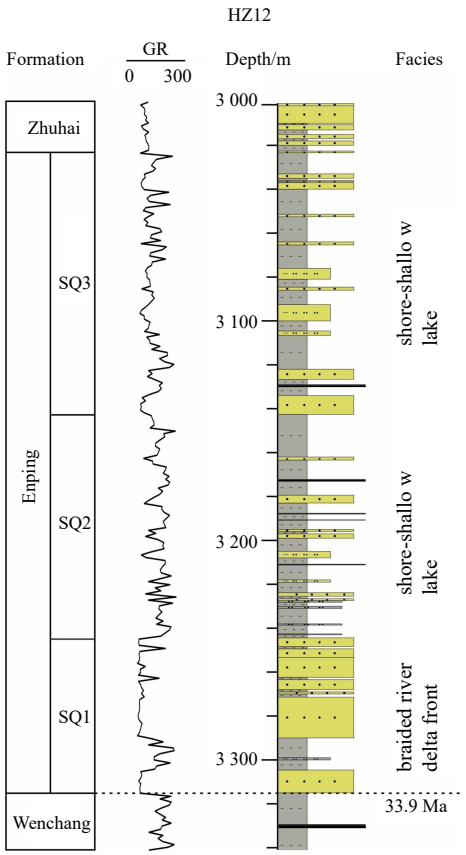

Fig. 2. Lithologic column of Enping Formation in Zhu Ⅰ Depression (HZ12).

acteristics of the coal seams include large numbers, thin single layer thicknesses, poor stability, and a wide distribution range. The distribution and development of the coal seams in the formation were affected by paleoclimate, paleogeography, paleostructure, and other factors. According to the available statistical data, the coal seams of the Enping Formation are mainly developed in the swamps of the lower plains of the braided river deltas and the coastal shallow lake. In this study, Well XJ of the Xijiang Sag, located in the central and western parts of the Zhu Ⅰ Depression, was selected as the study target. This sag is mainly developed in the shore-shallow lake facies, with braided river delta facies also developed, as detailed in Fig. 4. The Enping Formation was divided into upper (Part A) and lower (Part B) sections in this study. The obtained results were combined with the results of an orbital force study, as shown in Fig. 5. In the sag, the coal seams of Part A and Part B of the Enping Formation were mainly developed in the shore-shallow lake, marshes, and braided river delta facies. However, there were no coal seams observed in the fan delta facies. The distribution characteristics of the coal seams were consistent with the overall characteristics of the coal seam development of the Enping Formation, as shown in Figs 2 and 3.

3 Samples and methods

Natural gamma ray (GR) data of Well XJ in the Enping Formation were used for this study's analysis processes. Due to the existence of sedimentary discontinuities in most of the regions, Well XJ was selected as the study target. It was determined that Well XJ contained long-term lacustrine deposits and had a relatively complete strata, which were important for the examination of the potential influences of the orbital periods on the development of the thin coal seams in the Enping Formation. The data point interval of the GR logging curve was 0.125 m. The variations of coal seam ash production recorded by geophysical logging, such as gamma ray, density, and resistivity, were used to reflect the Milankovitch Cycles during the development of ancient peatland (Shao et al., 2022b). In addition, the intensity of the GR rays measured by the GR logging have been determined to be related to the radioactive isotopes of potassium, uranium, and thorium in mudstone, which reflect the content levels of organic matter in sediment and changes in paleoclimate (Zhao et al., 2021). Therefore, GR data can be used as alternative indicators of orbital force fluctuations in Earth records and are widely used in the analyses of paleoclimate and paleoenvironmental conditions (Wu et al., 2013). The Enping Formation and the underlying first member of the Wenchang Formation in Well XJ belong to relatively stable lacustrine deposits. The strata are relatively complete, which is conducive to the establishment of a more reliable astronomical time scale. The study target (Well XJ) was located in the main sub-sag of the Xijiang Sag. It was determined that the provenance supply mainly originated from the near-source provenance of the central uplift. The far-source provenance had little impact and no event flow effects were observed (Cheng, 2018).

The complexity of the geological environment of the Enping Formation affected the identification of the orbital signals to a certain extent. Therefore, a variety of methods were used to analyze the Enping Formation in this study in order to comprehensively determine the sediment rates and orbital signals. The data were first preprocessed using a detrending method to eliminate partrial environmental noise in the sediment records (Wu et al., 2011; Gong et al., 2005). The processed data were then subjected to multi-taper method (MTM) analysis (Thomson, 1982); evolutionary fast fourier transform (FFT) spectrum analysis (Kodama and Hinnov, 2014); and wavelet analysis processes. All three methods were utilized to identify the Milankovitch Cycles in the strata. correlation coefficient (COCO), and the evolutionary correlation coefficient (eCOCO) (Li et al., 2018), TimeOpt (time scale optimization) and eTimeOpt (evolutive time scale optimization) (Meyers, 2015, 2019) were used to comprehensively determine the sedimentation rates of each section. Then, the specific orbital signals were extracted using a Gaussian band-pass filtering method. The Milankovitch Cycles frequencies for the Oligocene timeframe were based on the theoretical La2004 astronomical solutions (Laskar et al., 2004). All of the analysis processes were conducted using Acycle v2.4.1 software (Li et al., 2019).

4 Results

As shown in Fig. 5, according to the analysis results of the overall lithology and sedimentation rate changes of Well XJ in the Enping Formation, the target area was divided into Part A (roughly corresponding to SQ2 and SQ3, equivalent to the first, second, and third members of the Enping Formation), and Part B (roughly corresponding to SQ1, equivalent to the fourth member of the Enping Formation).

Part A: After detrending the GR data in the depth range of Well XJ (Fig. 6a), COCO analysis (Fig. 7) and TimeOpt analysis (Fig. 8) were performed to determine the sedimentation rates. Both were iterated using 2 000 Monte Carlo simulations. In the COCO analysis, the optimal sedimentation rate in Part A was determined to 15.2 cm/ka according to the significance level of the H_0. In the TimeOpt analysis, the optimal sedimentation rate in Part A was 14.2 cm/ka (r^2_{opt} = 0.242 67, P-value = 0.019 5).

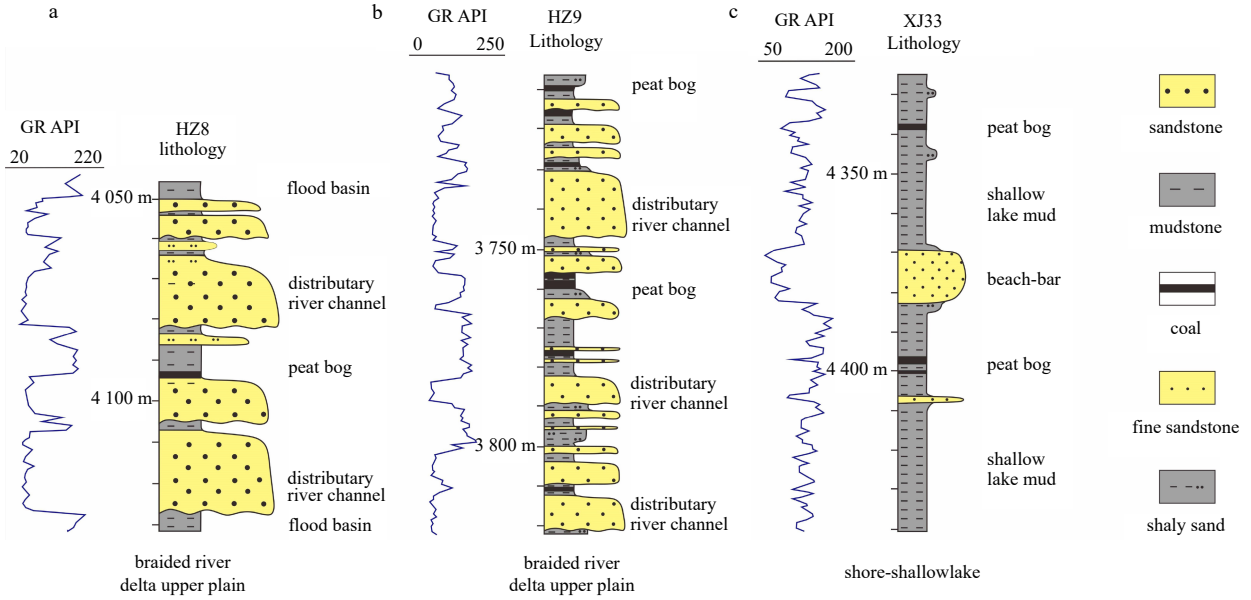

Fig. 3. Characteristics of coal-forming environments of Enping Formation in Zhu Ⅰ Depression. a. Upper plain of braided river delta of Enping Formation in Well HZ8. b. Lower plain of braided river delta of Enping Formation in Well HZ9. c. Shore-shallow lake of Enping Formation in Well XJ33.

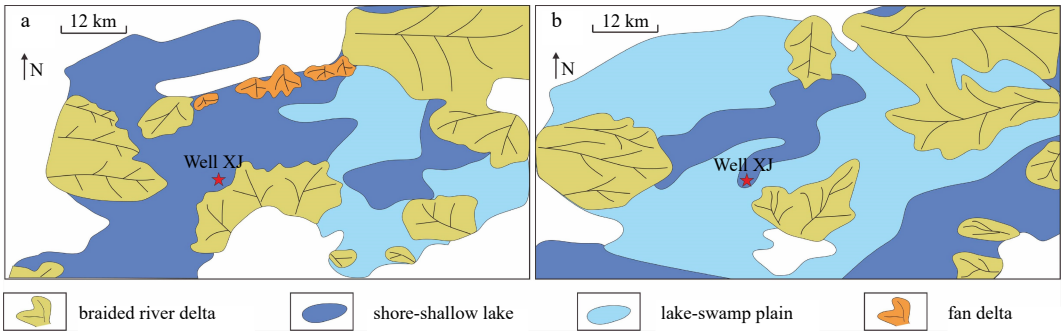

Fig. 4. Sedimentary facies distribution characteristics of Enping Formation in Xijiang Sag, Zhu Ⅰ Depression. a. Sedimentary facies distribution of the lower part of Enping Formation (Part B). b. Sedimentary facies distribution of the upper part of Enping Formation (Part A) (see Fig.1).

Subsequently, wavelet analysis (Fig. 6b), MTM analysis (Fig. 6c), and evolutionary FFT analysis (Fig. 6d) were performed. It was found that within the depth range of Well XJ, significant spectral peaks could be identified at 61 m, 50 m, 19.3 m, 18.1 m, 12.7 m, 4.5 m, 3.2 m, 2.8 m, 2.6 m, and 2.4 m, respectively, with confidence levels higher than 90% obtained for 61 m to 50 m, 19.3 m to 12.7 m, 4.5 m, and 3.2 m to 2.4 m. The ratios of the main cycle zone were close to those of the long eccentricity (405 ka); short eccentricity (125 ka and 95 ka); obliquity (40 ka); and precession (23.4 ka, 22.1 ka, 18.9 ka). Therefore, it was assumed that the cycle lengths were related to the Milankovitch Cycles of long orbital eccentricity, short orbital eccentricity, obliquity, and precession, respectively (Weedon, 2003).

In this research investigation, according to the optimal sedimentation rates obtained by the COCO and TimeOpt analyses, combined with the results of the MTM power spectrum analysis and the evolutionary FFT analysis, an approximate 61 m period corresponding to the long eccentricity period (405 ka) was identified.

Part B: After detrending the GR data in the depth range of Well XJ (Fig. 9a), COCO analysis (Fig. 8) and TimeOpt analysis (Fig. 10) were performed to determine the sedimentation rates. The results of the COCO analysis showed that the optimal sedimentation rate was 7.9 cm/ka, and the confidence level was higher than 99%. The TimeOpt analysis results showed that the optimal sedimentation rate was 7.7 cm/ka, and the confidence level was higher than 99.9%. Therefore, the results of the two analysis methods were similar.

Wavelet analysis (Fig. 9b), MTM analysis (Fig. 9c), and evolutionary FFT analysis (Fig. 9d) were subsequently performed. Within the depth range of Well XJ, significant spectral peaks were identified at 38 m, 31 m, 27 m, 10 m, 9.5 m, 7 m, 4.5 m, 3.4 m, 2.8 m, 2.6 m, and 2.4 m, and confidence levels were high at 38 m to 27 m, 10 m to 7 m, 4.5 m to 3.4 m, and 1.7 m to 0.8 m, respectively. The ratios of the main cycle zone were close to the long eccentricity (405 ka); short eccentricity (125 ka and 95 ka); obliquity (40 ka); and precession (23.4 ka, 22.1 ka, 18.9 ka). Therefore, it was considered that the lengths of those cycles were related to the Milankovitch Cycles of long orbital eccentricity, short orbital eccentricity, obliquity, and precession, respectively.

In the next investigative step, in accordance with the optimal sedimentation rates obtained by the COCO analysis and Time-

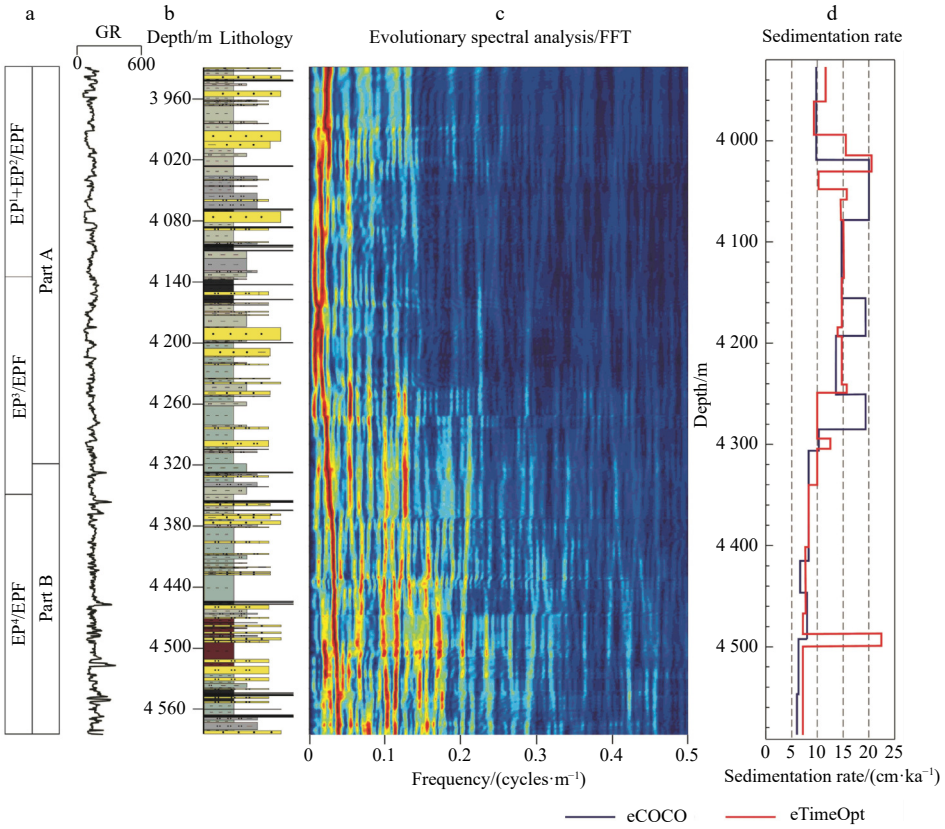

Fig. 5. The lithology, GR curve, evolutionary spectral analysis results, sedimentation rate curves and stratigraphic segmentation of Enping Formation in Well XJ. a. Sequence division and segmentation. b. Lithology and GR curve. c. Evolutionary spectral analysis results with a 100-m sliding window. d. Sedimentation rate curves obtained by eCOCO analysis and eTimeOpt analysis.

Opt analysis, combined with the results of the MTM power spectrum and evolutionary FFT analyses, an approximate 31 m period was identified that corresponded to the long eccentricity period (405 ka).

The representative long eccentricity (405 ka) and short eccentricity (125 ka) of the two parts were then filtered, and the GR data were converted from the depth domain to the time domain, as detailed in Fig. 11. It was determined that Part A spanned approximately 2.65 Ma, and Part B spanned approximately 3.5 Ma.

5 Discussion

5.1 *Control of the paleoenvironment of the coal seams*

The coal seams of the Enping Formation in the Zhu Ⅰ Depression have the characteristics of thinness and large numbers. The thicknesses of coal seams range mainly between 0 m and 2 m. At present, no thick coal seams have been found in the exploration results. When combined with the findings of previous studies, it was speculated that paleoclimate, paleostructure, and paleogeography factors had jointly controlled the accumulation and enrichment of peat in the Enping Formation.

The paleoplant types during the sedimentary period of the Enping Formation in the Zhu Ⅰ Depression included evergreen broad-leaved forest and vegetation, and broad-leaved species accounted for the majority (Guo, 2015). The content levels of *Polypodiaceaesporites* were generally higher during the sedimentary period of the Enping Formation, and the content levels of the hygrophyte species were higher than those of the xerophyte species. The ratio of hygrophyte species to xerophyte species was generally greater than 1, indicating that the paleoclimate of the Enping Formation had been a humid to semi-humid tropical-subtropical climate (Li , 2015). Previous studies have found that the expressions of the orbital periods from the Eocene to the Oligocene underwent a major switch, from eccentricity dominated to eccentricity-obliquity-precession dominated (Ao et al., 2020; Li et al., 2016b; Xu et al., 2023). Tardif et al. (2021) simulated the sensitivities of climate and vegetation to orbital forces during the late Eocene. The results suggested that the changes in the biome variations at low latitudes were tightly linked to the amounts of summer precipitation driven by the seasonal migration of the intertropical convergence zone (ITCZ) from 8 °N–30 °N in eastern Asia, which is mainly controlled by precession.

The sedimentary period of Enping Formation belongs to a late syn-rift phase that occurred during a fault-depression transformation stage (Zhang et al., 2014b). During that period, the basin had both the structural characteristics of a rift contraction period and the structural development pattern of the initial stage of the depressions (Li et al., 2016a; Zhang et al., 2014a). During the deposition of the Enping Formation, the tectonic activity gradually weakened, while the thermal subsidence increased during the initial stage of the depression. Subsequently, the Pearl (Zhujiang) River Mouth Basin entered a dominate depression stage (Peng et al., 2023b). In previous studies, it was considered that the middle and late stages of rift basin evolution were the main periods of the development of the coal seams in this type of basin (Zhu et al., 2022). Since the development of coal seams during the sedimentary periods of the Enping Formation were relatively common, the existence of stable tectonic environmental condi-

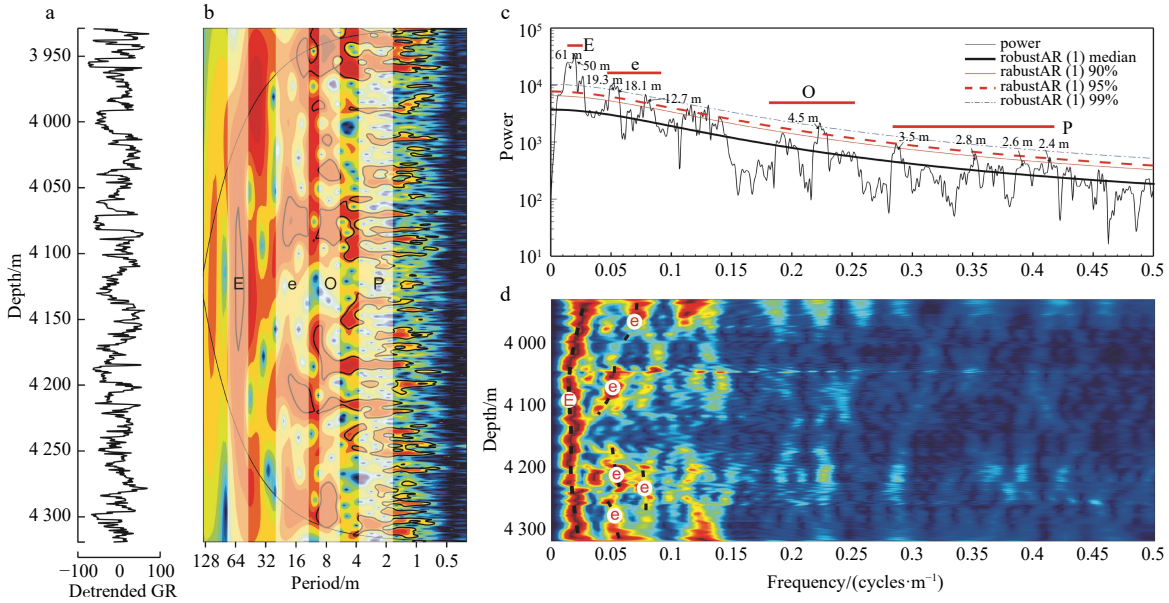

Fig. 6. Orbital signal recognition in Part A of Enping Formation. a. GR curve after detrending. b. Wavelet analysis. c. Multi-taper method power spectrum analysis. d. Evolutionary spectral analysis results with a 90-m sliding window.

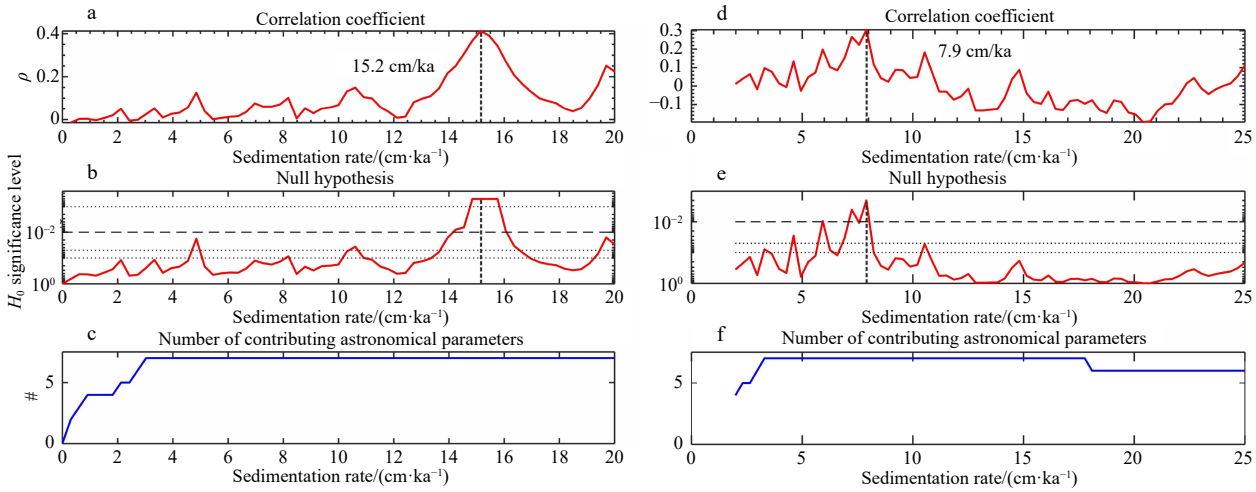

Fig. 7. Optimal sedimentation rates in Part A and B of Enping Formation by COCO analysis. a. The correlation coefficient in Part A is higher at 15.2 cm/ka. b. Part A null hypothesis confidence, less than 0.001 at 15.2cm/ka. c. The number of astronomical parameters contributed by Part A in the test of sedimentation rate is 7 at 15.2 cm/ka. d. The correlation coefficient of Part B is higher value at 7.9 cm/ka. e. Part B null hypothesis confidence, less than 0.01 at 7.9 cm/ka. f. The number of astronomical parameters contributed by Part B in the test of sedimentation rate is 7 at 7.9 cm/ka.

tions during those periods was indicated. The several separate sags or semi-grabens developed in the Zhu Ⅰ Depression with high rift rates (maximum value of 200 m/Ma) formed a variety of graben-type and semi-graben-type coal accumulations (Li and Rao, 1994; Morley, 2016). From the perspectives of the seismic and drilling data, the secondary uplifts (depression uplifts) under the background of the depressions, and the secondary depressions (uplift depressions) under the background of the uplifts, are considered to be conducive to coal formation (Yin, 2022).

The Enping Formation in the Zhu Ⅰ Depression was formed under the effects of multiple sources, such as the Northern Uplift Zone, Dongsha Uplift, and the low uplifts in the sag. The sedimentary environments were dominated by braided river deltas and lacustrine facies (Cao, 2021; Guo et al., 2013), which provided a wide range of favorable coal-forming zones. As determined in previous related studies, according to the differences in lithology, the Enping Formation can be divided into two parts: the top (Part A) and the bottom (Part B). Part A is mainly composed of a sand-mudstone interbed, while Part B includes thick mudstone with a scattering of thin coal seams (Fu et al., 2021). In addition, the Enping Formation can be divided into three third-order sequences, as shown in Fig. 2. The lake in the SQ1 period was relatively shallow, mainly developing from braided river deltas, fan deltas, and shore-shallow lake environments. During the SQ2 period, the water body expanded, and the braided river deltas and shallow lake environments had expanded significantly when compared with the SQ1 period. However,

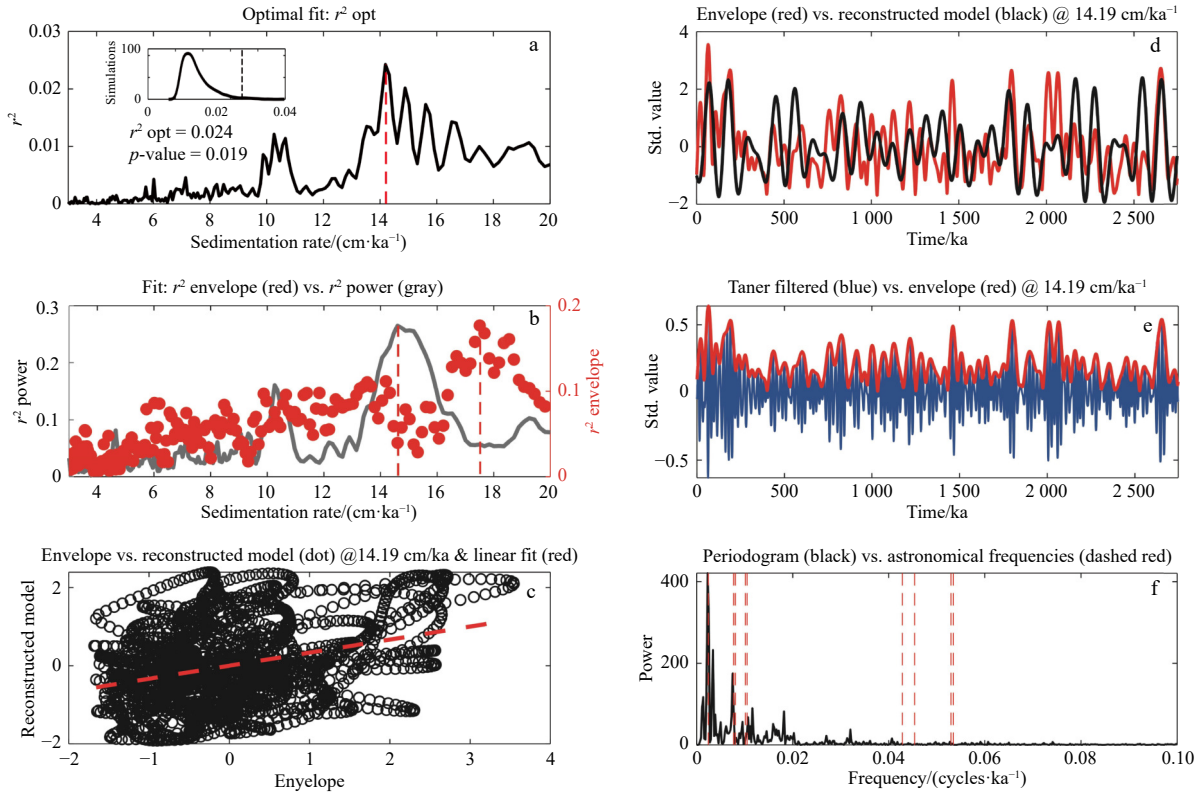

Fig. 8. TimeOpt analysis in Part A of Enping Formation. a. Combined envelope and spectral power fit (r^2_{opt}) at each evaluated sedimentation rate and the summary of 2 000 Monte Carlo simulations, p-value = 0.019 5. b. The squared Pearson correlation coefficient ($r^2_{envelope}$; red) and spectral power fitting correlation coefficient (r^2_{power}; gray). c. Cross plot of the data amplitude envelope and the TimeOpt-reconstructed eccentricity model in panel "d"; dashed red line is the 1:1 line. d. Comparison of data amplitude envelope (red) and TimeOpt reconstructed eccentricity model (black). e. Comparison of band-pass precession signal (blue) with data amplitude envelope (red). f. Periodogram of the data. The red dotted line indicates the target period of eccentricity and precession.

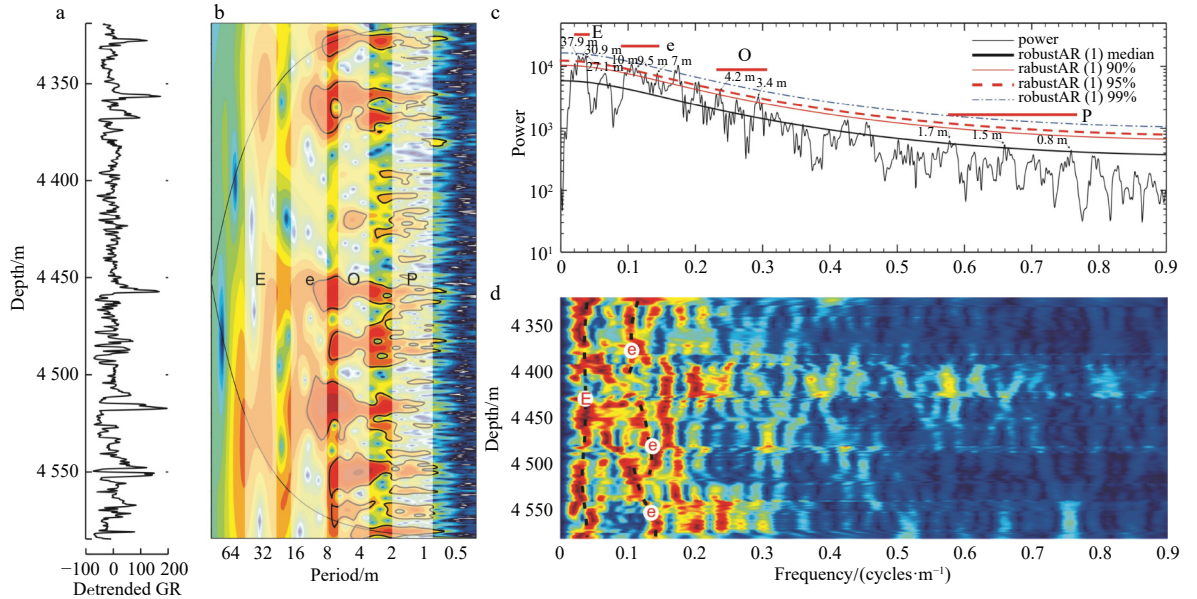

Fig. 9. Orbital signal recognition in Part B of Enping Formation. a. GR curve after detrending. b. Wavelet analysis. c. Multi-taper method power spectrum analysis. d. Evolutionary spectral analysis results with a 60-m sliding window.

during the SQ3 period, the lake began to shrink, and braided river delta deposits were widely developed in the basin (Yin, 2022). In general, the coal-forming environmental conditions of the SQ1 to SQ3 periods in the Enping Formation were characterized by braided river delta lower plains, braided river delta fronts, and shore-shallow lake environments.

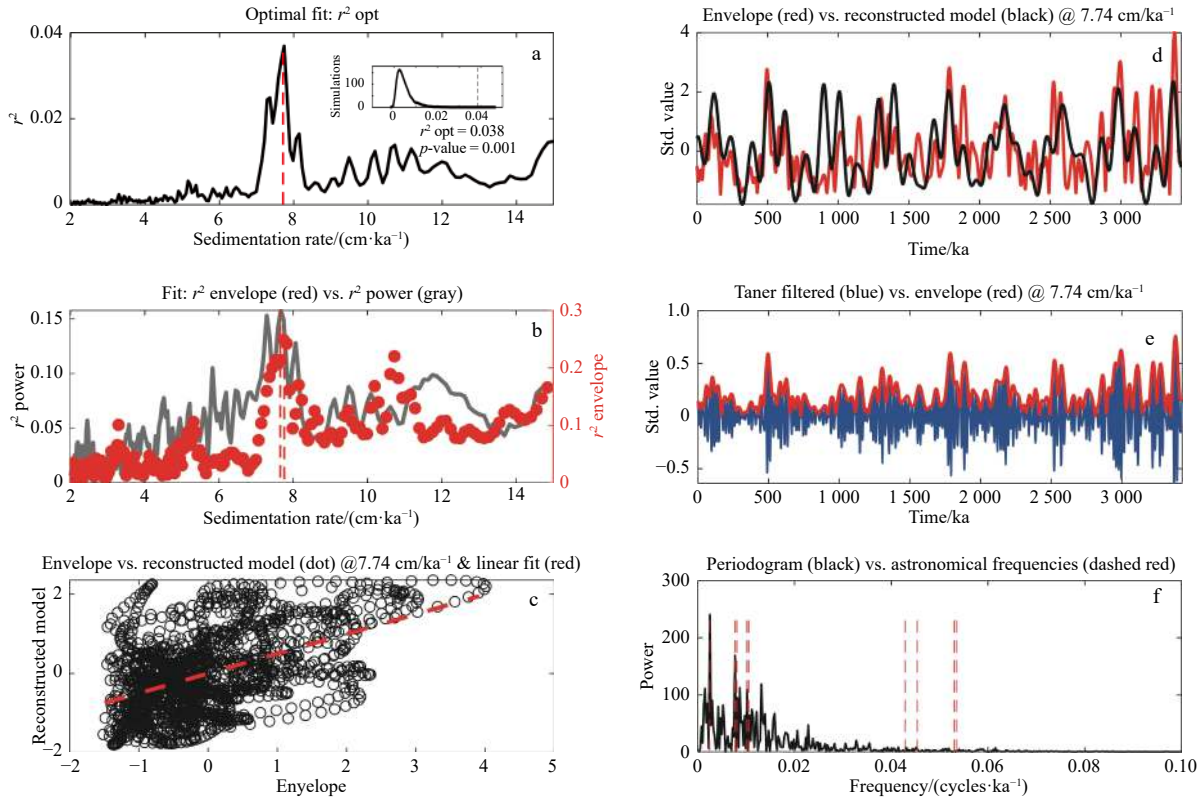

Fig. 10. TimeOpt analysis in Part B of Enping Formation. a. Combined envelope and spectral power fit (r^2_{opt}) at each evaluated sedimentation rate and the summary of 2 000 Monte Carlo simulations, *p*-value = 0.001. b. The squared Pearson correlation coefficient ($r^2_{envelope}$; red) and spectral power fitting correlation coefficient (r^2_{power}; gray). c. Cross plot of the data amplitude envelope and the TimeOpt-reconstructed eccentricity model in panel "d"; dashed red line is the 1:1 line. d. Comparison of data amplitude envelope (red) and TimeOpt reconstructed eccentricity model (black). e. Comparison of band-pass precession signal (blue) with data amplitude envelope (red). f. Periodogram of the data. The red dotted line indicates the target period of eccentricity and precession.

5.2 *Influence of orbital forces on coal accumulation*

The research results obtained in many regions have shown that the development of coal seams is significantly affected by orbital forces. Due to the lack of an absolute age limit, a floating astronomical time scale was constructed to an orbit of 405 ka. The obvious peak signals of long eccentricity, short eccentricity, obliquity, and precession were identified in the spectrum analysis results, and the corresponding frequency groups and cycle lengths were obtained. After filtering the corresponding signal frequency, the filtering results were compared with the lithology in the depth domain, and the positions of the corresponding coal seams were marked on the filter curves, as detailed in Figs 12 and 13. The results showed that the coal seams of the Paleogene Enping Formation in the PRMB region had been significantly affected by orbital forces. It was determined that the majority of the coal seams developed during a period with a high value of short eccentricity, which corresponded well with the low value of the precession. The occurrences of continuous multi-layered thin coal seams were highly correlated with the precession period and the high-value short eccentricity period, and the coal seam interval was similar to the precession period. Those results were very similar to the Pliocene Lupoaia lower section of the Oltenia Basin (near the City of Motru), as well as south-west Romania. The Lupoaia Pliocene lower cycle lignite corresponded to the high-value period of eccentricity corresponding to a warm period (interglacial period). However, due to the unclear understanding of the precession phenomena in the area, the influencing effects of the precession on the formation of the coal seams has not yet been explored (van Vugt et al., 2001). In previous studies of the Pinghu Formation in the Xihu Sag, which belongs to the Paleogene, the o btained results of the obliquity and precession controls of the formation of thin coal seams were successfully obtained. The results were similar to previous findings that suggested that low precession corresponds to the development of thin coal seams (Zhao et al., 2022). Therefore, when combined with the relatively cold climate conditions of the early Oligocene, it is reasonable to assume the characteristics of coal formation during periods of minimum precession will differ from the coal formation during periods of high eccentricity (warm and humid periods with strong summer insolation) (van Vugt et al., 2000, 2001).

Previous research results have also indicated that lacustrine deposition records orbital periods by regulating the monsoon systems affecting lake level fluctuations (Kashiwaya et al., 2001; Valero et al., 2014). For example, periods of high eccentricity tend to have strong seasonal contrast, during which the atmospheric precipitation generally increases and climate conditions are humid. However, during periods of low eccentricity, the seasonal contrast tends to be low and the climatic conditions stable (Noorbergen et al., 2018; Zhang et al., 2020b). During the deposition period of the Enping Formation, the warm and humid climate that existed during the periods of high eccentricity were favorable for the development of peatland. However, during the periods of low eccentricity, the climate conditions were cold and

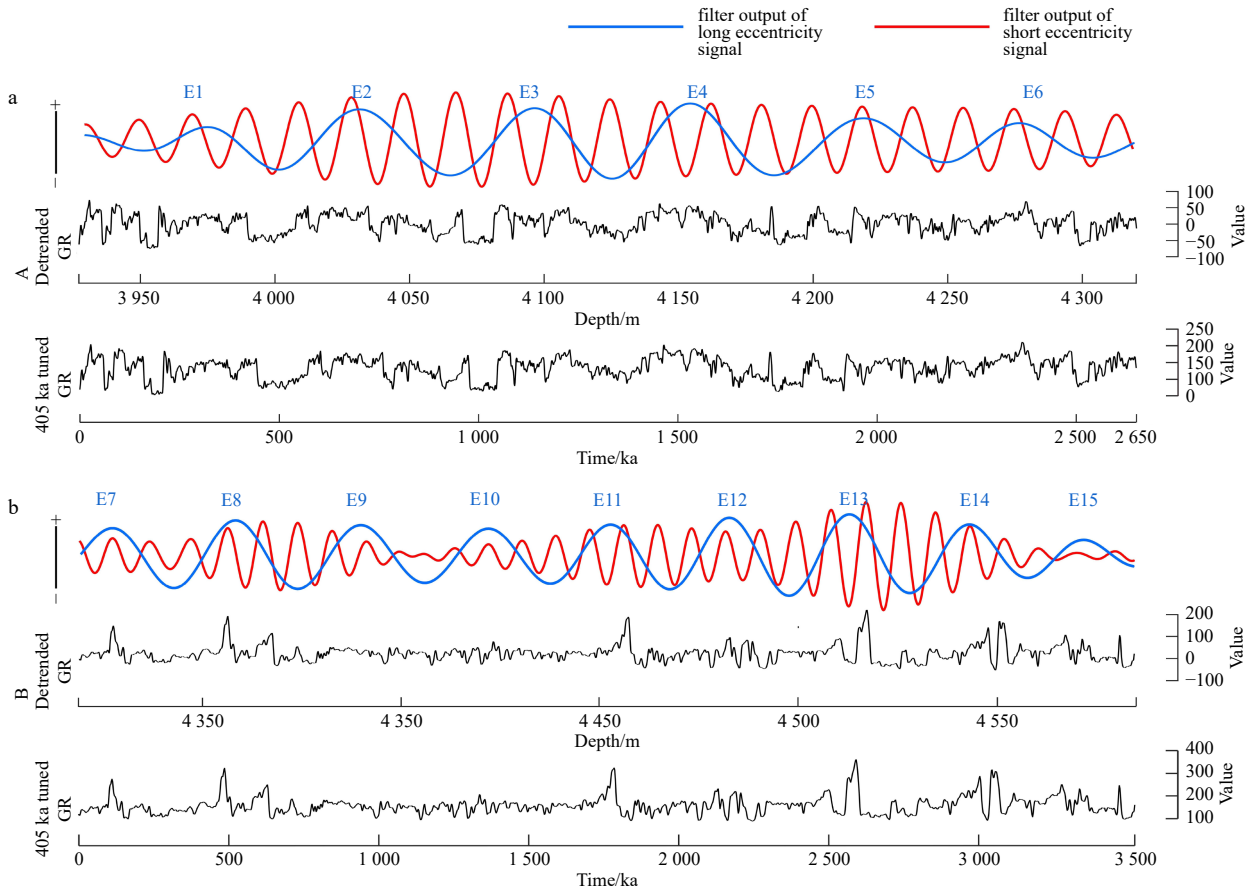

Fig. 11. The filtering results of long eccentricity (blue) and short eccentricity (red) in Part A and Part B of Enping Formation. a. Filtering results, detrended GR data in the depth domain, and the GR time series of the GR depth record converted to the time domain of Part A. b. Filtering results, detrended GR data in the depth domain, and the GR time series of the GR depth record converted to the time domain of Part B.

dry and large amounts of detrital material were deposited, which was not conducive to peat accumulation (van Vugt et al., 2000, 2001; Liu et al., 2020). Those factors resulted in the Enping Formation coal seam formation being concentrated in the periods with high eccentricity values.

Eccentricity controls the seasonal variations of insolation by tuning precession (Berger et al., 1992; Laskar et al., 2004; Bosmans et al., 2018). During the periods with high eccentricity, the seasonality of the Northern Hemisphere is strong and the precession is low, such as during the summer solstice. The Northern Hemisphere can be affected by strong insolation, high temperatures, and increased monsoon rainfall (Kashiwaya et al., 2001; Olsen and Kent, 1996; Valero et al., 2014). Previously, in such warm and humid climate environments with strong insolation, peat swamps continued to develop and coal was formed. However, when the precession gradually shifted from low to high, the climate conditions became drier. At such times, the perihelion was in the winter solstice, and the seasonal variations were weakened (Vázquez et al., 2000; Bosmans et al., 2018). The environmental climate was not suitable for the development of peat swamps and peatlands gradually disappeared, resulting in thinner and fewer coal seams during the periods of low precession. During periods of low eccentricity, the climate conditions are relatively stable. The rainfall and insolation tend to be reduced, and the fluctuations of the precession have little effect on the climate conditions. In addition, the seasonal changes become weakened (Rollins et al., 1993), which is not conducive to coal formation. In this study, the occurrences of two consecutive layers of coal between 4 060 m and 4 080 m in the study area were determined to have not been strictly controlled by the two precession periods (Fig. 12b). Alternatively, it was considered that the two layers of coal corresponded to the low values of the same precession period, and it was speculated that other reasons may have caused the middle thin layer of the mudstone bed.

5.3 *Theoretical model for climatically controlled coal deposition in the Enping Formation*

During the sedimentary period of the Enping Formation, the mode of the orbital forcing climate controlling the formation of the coal seams was different from that of the low eccentricity periods (Zhang et al., 2020b). It was speculated that the orbital parameters controlling the development of the coal seams had varied during the different periods and under different environmental conditions (van Vugt et al., 2001). The periods of high eccentricity were conducive to coal formation, and the short eccentricity cycles contained 4 to 5 precession cycles. Therefore, based on the results obtained in this study, a theoretical model that could be divided into five stages (Stage 1 to Stage 5) was established in order to determine the influencing effects of short eccentricity and precession forces under the climate conditions during the Paleogene that potentially affected the development of coal seams and the formation of peat swamps (Fig. 14). The five stages of the model were as follows:

Stage 1: When the eccentricity increased, the seasonal con-

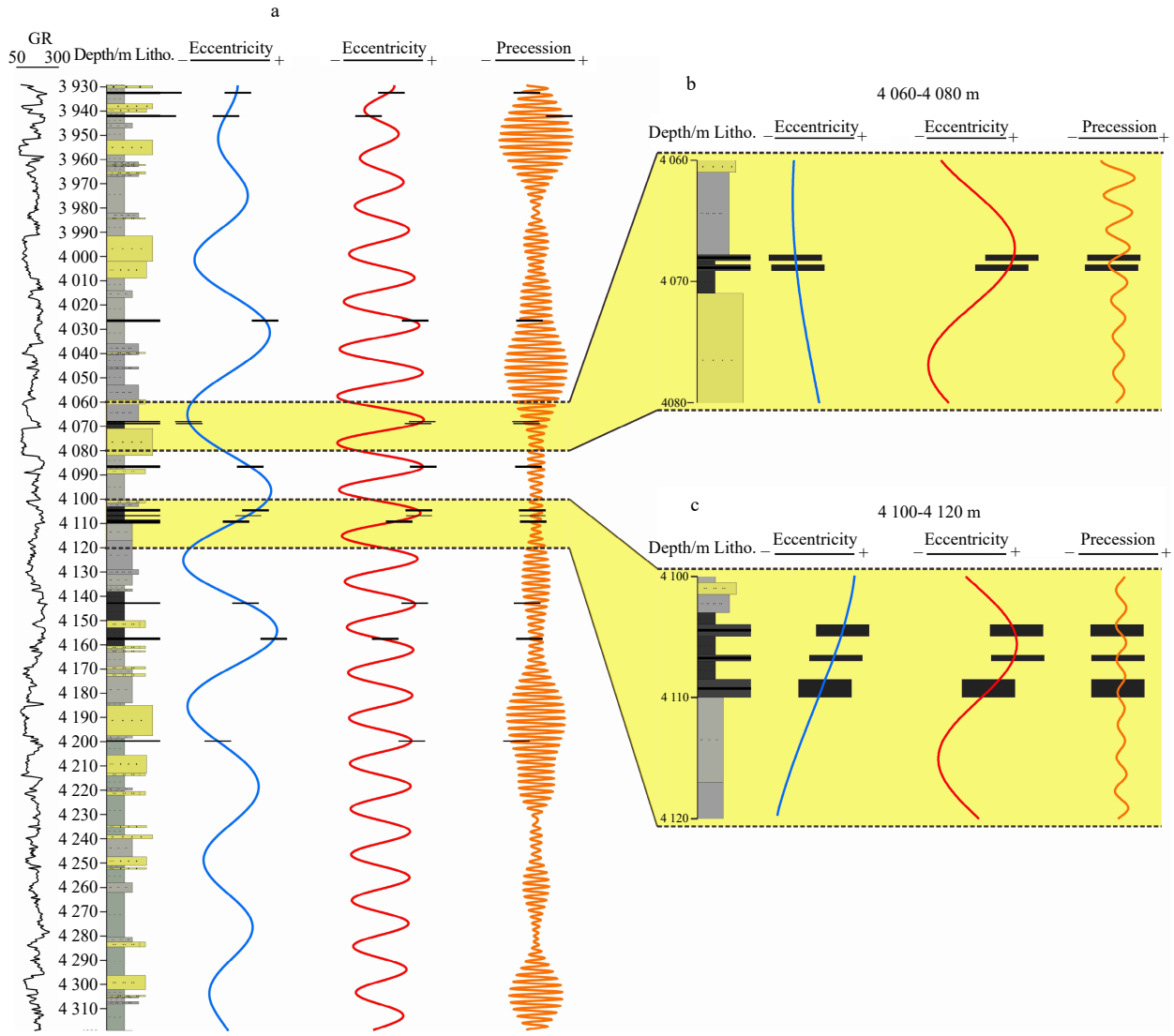

Fig. 12. The relationship between lithology and eccentricity and precession filter curves in Part A of Enping Formation. a. Comparison of GR curve and lithology with long eccentricity (blue), short eccentricity (red), and precession (yellow) filter curves in the depth domain. b. Comparison of continuous multi-layer thin coal seams and filter curves in depth domain in 4 060-4 080 m. c. Comparison ofcontinuous multi-layer thin coal and filter curves in depth domain in 4 100–4 120 m.

trast increased. During the periods of low precession, the perihelion of the Northern Hemisphere was in a summer solstice stage. At that time, the insolation became stronger, along with the atmospheric precipitation. The climate became humid, vegetation became denser, and peat accumulation was enhanced (Fig. 14c).

Stage 2: When the eccentricity increased and the precession was high, the Northern Hemisphere perihelion appeared at the winter solstice. The climate was dry and cold, and the sediment supplies increased. At that time, the accumulation of peat ceased, and the peat was deposited (Fig. 14d).

Stage 3: During the periods with high eccentricity, the Northern Hemisphere received maximum insolation when the precession was low. The atmospheric precipitation was rich, and the vegetation was abundant. The large areas of peat swamp that developed were conducive to the formation of thin coal seams (Fig. 14e).

Stage 4: When the eccentricity decreased and the precession was high, the Northern Hemisphere had the characteristics of weak insolation and low atmospheric precipitation. Peat swamps rarely developed during such periods. As the sediment increased, the coal seams formed in Stage 3 were buried (Fig. 14f).

Stage 5: During the periods characterized with decreasing eccentricity, it has been determined that when the precession was low, the Northern Hemisphere received stronger insolation and atmospheric precipitation, similar to Stage 1 (Fig. 14g).

In Fig. 14, the stages denoted as a, b, i, and h are in periods of low eccentricity were not favorable for coal formation. Few coal seams were developed during those stages. For the formation of the thicker coal seams, it was determined that the precession during the periods of high eccentricity had affected the periodic changes of the coal macerals (Shao et al., 2022a).

6 Conclusions

The relationships between the thin coal seams and the astronomical orbital periods of the Enping Formation in the northern section of the SCS were analyzed in this study. The results provide new insights into the influencing effects of the orbital periods of the Paleogene on the development of thin coal seams

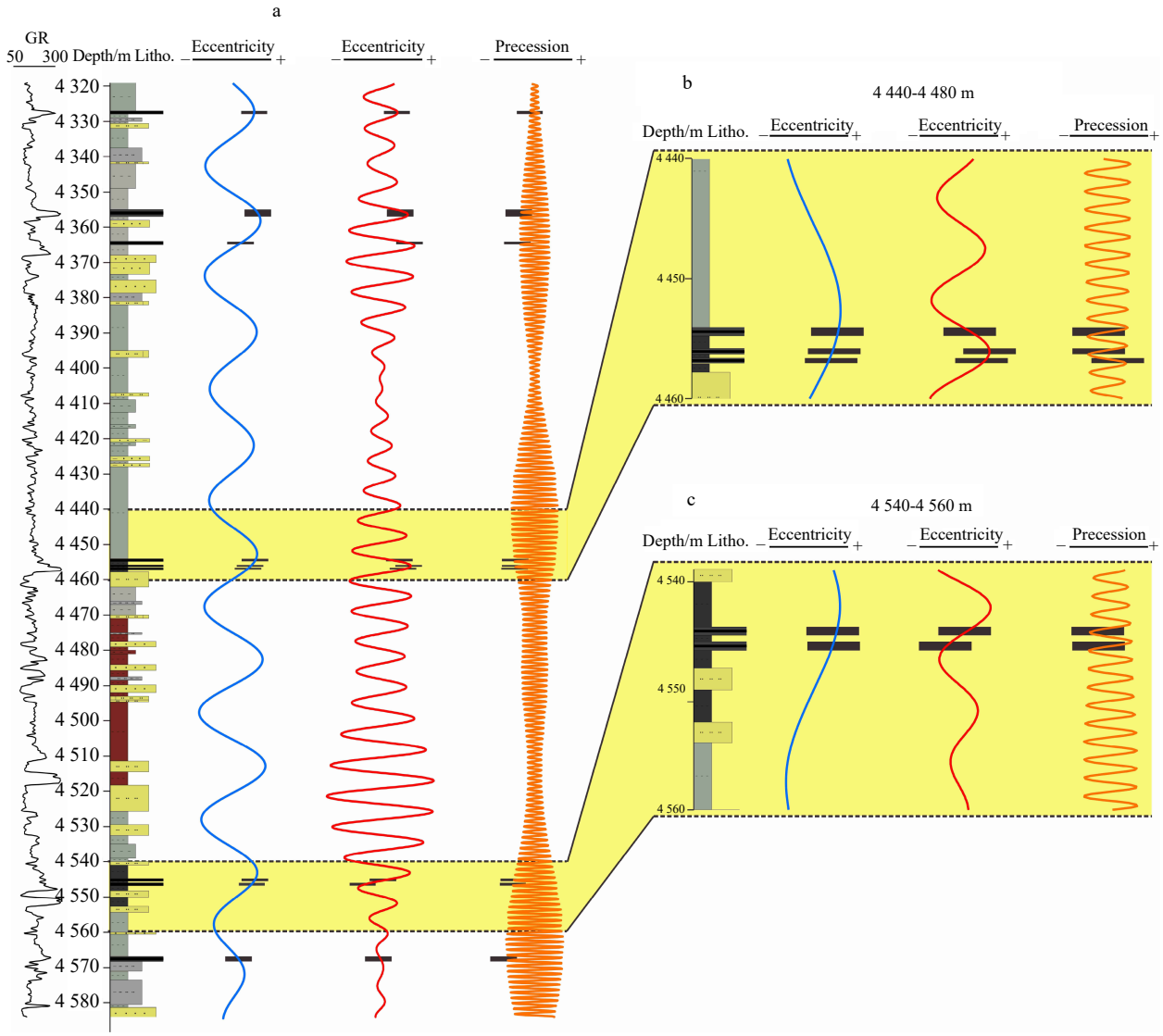

Fig. 13. The relationship between lithology and eccentricity and precession filter curves of Enping Formation Part B. a. Comparison of GR curve and lithology with long eccentricity (blue), short eccentricity (red), and precession (yellow) filter curves in the depth domain. b. Comparison of 4 440–4 470 m continuous multi-layer thin coal and filter curves in depth domain. c. Comparison of 4 540–4 560 m continuous multi-layer thin coal and filter curves in depth domain.

in the region. The conclusions reached in this study were summarize as follows:

(1) The long eccentricity (405 ka) of the relatively complete lacustrine strata of Well XJ in the Enping Formation was filtered, and an astronomical time scale was established. The results showed that the Enping Formation spanned approximately 6.15 Ma±, from 33.9 Ma± to 27.75 Ma±, respectively.

(2) A comparison was made between the filter curves of the short eccentricity of Well XJ in the Enping Formation and the coal seams in the depth domain. It was considered that the short eccentricity had a strong influence on the development of the coal seams, with the coal seams being mainly developed during the high value periods of short eccentricity. In addition, by comparing the filter curves of the precession with the distribution of the coal seams, it was determined that the thin coal seams corresponded well to the low values of the precession. The occurrence of continuous multi-layered coal during the periods of high values of short eccentricity corresponded to the intervals of the low values of the precession. Therefore, based on the determined influencing effects of the orbital periods on the climate and environmental conditions, it was speculated that the precession periods were the main astronomical orbital factors that caused the multi-staged development of the Paleogene thin coal seams.

(3) A theoretical model of peat formation affected by short eccentricity and precession force climatic conditions during the Paleogene was established in this study through comprehensive analysis processes. The proposed model revealed the influencing effects of the patterns of the Paleogene astronomical cycles and the paleoclimate evolution on the development of the thin coal-seam groups in China's offshore lacustrine basins.

Acknowlegements

We thank the Beijing Research Center of CNOOC (China) Co., Ltd. for providing the data used in this study. We would like to express our sincere appreciation to Dr. Song Cuiyu and Dr. Zhang Zhihui from Shandong University of Science and Technology, and Master Wen He from China University of Mining & Technology, Beijing, for their assistance. We specially thank the three an-

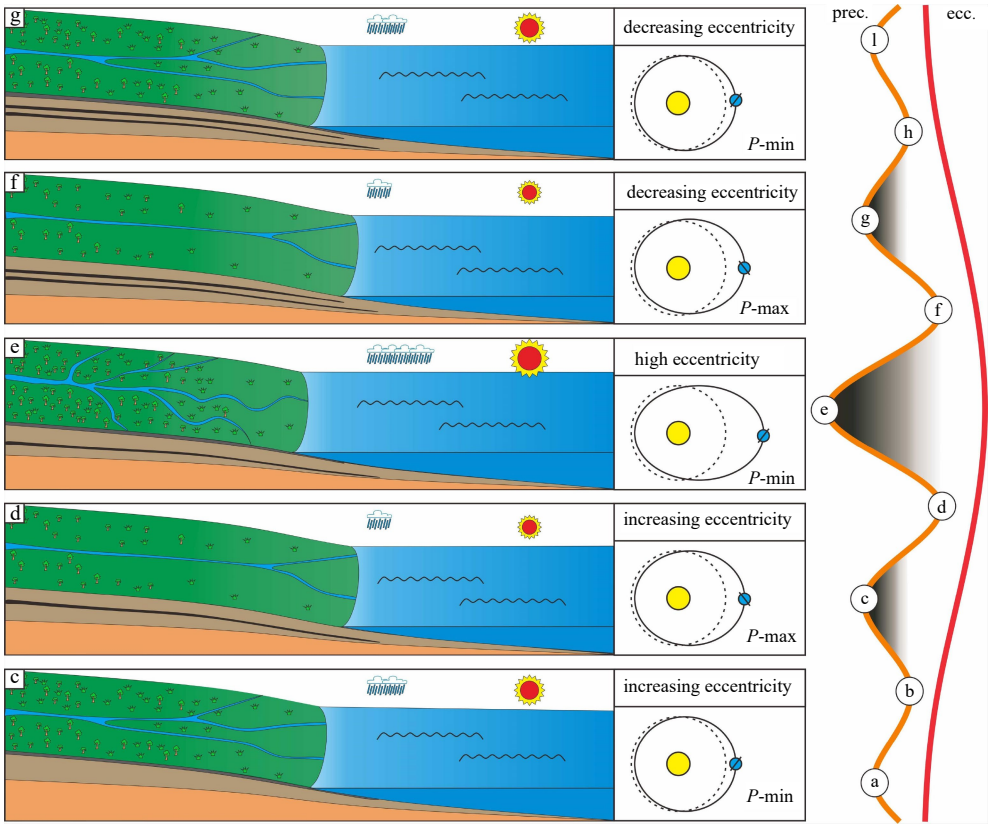

Fig. 14. The theoretical model of short eccentricity (red) and precession (yellow) forcing climate control formed by peat is explained in five stages.

onymous reviewers for their critical comments and suggestions, which significantly improved this presentation.

References

Abels H A, Aziz H A, Krijgsman W, et al. 2010. Long-period eccentricity control on sedimentary sequences in the continental Madrid Basin (middle Miocene, Spain). Earth & Planetary Science Letters, 289(1–2): 220–231

Ao H, Dupont-Nivet G, Rohling E J, et al. 2020. Orbital climate variability on the northeastern Tibetan Plateau across the Eocene-Oligocene transition. Nature Communications, 11(1): 5249, doi: 10.1038/s41467-020-18824-8

Berger A, Loutre M F, Laskar J. 1992. Stability of the astronomical frequencies over the Earth's history for paleoclimate studies. Science, 255(5044): 560–566, doi: 10.1126/science.255.5044.560

Boulila S, Galbrun B, Miller K G, et al. 2011. On the origin of Cenozoic and Mesozoic "third order" eustatic sequences. Earth-science reviews, 109(3–4): 94–112, doi: 10.1016/j.earscirev.2011.09.003

Bosmans J H C, Erb M P, Dolan A M, et al. 2018. Response of the Asian summer monsoons to idealized precession and obliquity forcing in a set of GCMs. Quaternary Science Reviews, 188: 121–135, doi: 10.1016/j.quascirev.2018.03.025

Boucot A J, Xu C, Scotese C R, et al. 2013. Phanerozoic paleoclimate: An atlas of lithologic indicators of climate. In: SEPM Concepts in Sedimentology and Paleontology. SEPM Society for Sedimentary Geology

Cao Qinming. 2021. Formation mechanism of middle-deep sandstone reservoir of Eocene in Zhu Ⅰ Depression, Pearl River Mouth Basin (in Chinese)[dissertation]. Chengdu: Chengdu University of Technology

Cheng Yuan. 2018. Study on semi-quantitative prediction model on sensitive parameters of "source to sink" system in continental basin (in Chinese)[dissertation]. Wuhan: China University of Geosciences

Cheng Shixiu, Li Sanzhong, Suo Yanhui, et al. 2012. Cenozoic tectonics and dynamics of basin groups of the Northern South China Sea. Marine Geology & Quaternary Geology (in Chinese), 32(6): 79–93

Fu Chao, Li Shengli, Li Shunli, et al. 2021. Spatial and temporal variability of sediment infilling and episodic rifting in the North Pearl River Mouth Basin, South China Sea. Journal of Asian Earth Sciences, 211: 104702, doi: 10.1016/j.jseaes.2021.104702

Gong Yiming, Xu Ran, Tang Zhongdao, et al. 2005. The Upper Devonian orbital cyclostratigraphy and numerical dating conodont zones from Guangxi, South China. Science in China Series D:Earth Sciences, 48(1): 32–41, doi: 10.1360/03yd0025

Guo Pengfei. 2015. Formation mechanism of high-quality source rock and its contribution to hydrocarbon accumulation in Zhuyi Depression, Pearl River Mouth Basin (in Chinese)[dissertation]. Wuhan: China University of Geosciences

Guo Qiaozhen, Chen Feng, Yang Xianghua, et al. 2013. Shallow braided deltaic system in Enping formation of Huizhou Depression, Pearl River Mouth. Marine Geology & Quaternary Geology (in Chinese), 33(1): 25–32

Galeotti S, Deconto R, Naish T, et al. 2016. Antarctic Ice Sheet variability across the Eocene-Oligocene boundary climate transition. Science, 352(6281): 76–80, doi: 10.1126/science.aab0669

Hinnov L A. 2013. Cyclostratigraphy and its revolutionizing applications in the earth and planetary sciences. Geological Society of America Bulletin, 125(11–12): 1703–1734, doi: 10.1130/B30934.1

Huang Lüsheng. 1999. Tertiary biostratigraphic framework of Pearl River Mouth Basin. China Offshore Oil and Gas (Geology) (in Chinese), 13(6): 406–415

Huang Lüsheng, Zhong Bizhen. 1998. New materials of the calcareous nannofssil in the middle Eocene Wenchang Formation from the Pearl River Mouth Basin. China Offshore Oil and Gas (Geology) (in Chinese), 12(1): 31–35

Husinec A, Read J F. 2018. Cyclostratigraphic and $\delta^{13}C$ record of the Lower Cretaceous Adriatic platform, Croatia: Assessment of

Milankovitch-forcing. Sedimentary Geology, 373: 11–31, doi: 10.1016/j.sedgeo.2018.05.010
Jiang Hua, Wang Hua, Li Junliang, et al. 2009. Research on hydrocarbon pooling and distribution patterns in the Zhu-3 Depression, the Pearl River Mouth Basin. Oil & Gas Geology (in Chinese), 30(3): 275–281,286
Kashiwaya K, Ochiai S, Sakai H, et al. 2001. Orbit-related long-term climate cycles revealed in a 12-Myr continental record from Lake Baikal. Nature, 410(6824): 71–74, doi: 10.1038/35065057
Kodama K P, Hinnov L A. 2014. Rock Magnetic Cyclostratigraphy. New Jersey: Wiley-Blackwell
Laskar J, Robutel P, Joutel F, et al. 2004. A long-term numerical solution for the insolation quantities of the earth. Astronomy and Astrophysics, 428(1): 261–285, doi: 10.1051/0004-6361:20041335
Lei Zuoqi. 1993. Discussion on the age assignment of Enping Formation in the Pearl River Mouth basin. Journal of Stratigraphy (in Chinese), 17(2): 108–114
Li Shaojie. 2015. Study on the formation modes of coal-measure source rocks in northern basins of South China Sea (in Chinese) [dissertation]. Wuhan: China University of Geosciences
Li Mingsong, Hinnov L, Kump L. 2019. *Acycle*: Time-series analysis software for paleoclimate research and education. Computers & Geosciences, 127: 12–22
Li Bangyong, Huang Chuanyan, Zhang Hongwei, et al. 2016a. Provenance system characters of fault-depressed transforming period: Insights from the third member of Dongying formation in Baxian Sag. Geological Science and Technology Information (in Chinese), 35(3): 56–64
Li Y X, Jiao W J, Liu Z H, et al. 2016b. Terrestrial responses of low-latitude Asia to the Eocene-Oligocene climate transition revealed by integrated chronostratigraphy. Climate of the Past, 12(2): 255–272, doi: 10.5194/cp-12-255-2016
Li Mingsong, Kump L R, Hinnov L A, et al. 2018. Tracking variable sedimentation rates and astronomical forcing in Phanerozoic paleoclimate proxy series with evolutionary correlation coefficients and hypothesis testing. Earth and Planetary Science Letters, 501: 165–179, doi: 10.1016/j.epsl.2018.08.041
Li Zengxue, Liu Ying, Li Xiaojing, et al. 2022. The control of Paleogene peat swamp destruction and reconstruction on the formation of coal-type source material in the Qiongdongnan Basin. Oil & Gas Geology (in Chinese), 43(6): 1309–1320
Li Zhenxiong, Ma Junrong. 1992. Polynological assemblages of Enping formation in the Pearl River Mouth. Acta Petrolei Sinica (in Chinese), 13(2): 258–267
Li Pinglu, Rao Chuntao. 1994. Tectonic characteristics and evolution history of the Pearl river mouth basin. Tectonophysics, 235 (1–2): 13–25, doi: 10.1016/0040-1951(94)90014-0
Li Sanzhong, Suo Yanhui, Liu Xin, et al. 2012a. Basin dynamics and basin groups of the South China Sea. Marine Geology & Quaternary Geology (in Chinese), 32(6): 55–78
Li Zengxue, Zhang Gongcheng, Li Ying, et al. 2012b. The Paleogene coal-bearing basin and coal-measures distribution of China sea area. Earth Science Frontiers (in Chinese), 19(4): 314–326
Liu Wei, Wu Huaichun, Hinnov L A, et al. 2020. An 11 million-year-long record of astronomically forced fluvial-alluvial deposition and paleoclimate change in the Early Cretaceous Songliao synrift basin, China. Palaeogeography, Palaeoclimatology, Palaeoecology, 541: 109555
Meyers S R. 2015. The evaluation of eccentricity-related amplitude modulation and bundling in paleoclimate data: An inverse approach for astrochronologic testing and time scale optimization. Paleoceanography, 30(12): 1625–1640, doi: 10.1002/2015PA002850
Meyers S R. 2019. Cyclostratigraphy and the problem of astrochronologic testing. Earth-Science Reviews, 190: 190–223, doi: 10.1016/j.earscirev.2018.11.015
Morley C K. 2016. Major unconformities/termination of extension events and associated surfaces in the South China Seas: Review and implications for tectonic development. Journal of Asian Earth Sciences, 120: 62–86, doi: 10.1016/j.jseaes.2016.01.013
Noorbergen L J, Abels H A, Hilgen F J, et al. 2018. Conceptual models for short-eccentricity-scale climate control on peat formation in a lower Palaeocene fluvial system, north-eastern Montana (USA). Sedimentology, 65(3): 775–808, doi: 10.1111/sed.12405
Olsen P E, Kent D V. 1996. Milankovitch climate forcing in the tropics of Pangaea during the Late Triassic. Palaeogeography, Palaeoclimatology, Palaeoecology, 122(1–4): 1–26
Peng Guangrong, Chen Weitao, Jia Peimeng, et al. 2023a. Middle-late Eocene climate in the Pearl River Mouth Basin: Evidence from a palynological and geological element record in the Xijiang main subsag. Minerals, 13(3): 374, doi: 10.3390/min13030374
Peng Guangrong, Long Zulie, Shi Yuling, et al. 2022. Discussion on integrated geological and geophysical identification method for spatial distribution of favorable source rocks in depression with lack of drilling data: a case study of Enping 17 Sag, Zhu Ⅰ Depression, Pearl River Mouth Basin. Petroleum Geology & Experiment (in Chinese), 44(6): 1116–1122
Peng Guangrong, Zhang Lili, Xu Xinming, et al. 2023b. Core complex and detachment structure in the Kaiping Sag, Pearl River Mouth Basin and a discussion on the dynamics. Earth Science (in Chinese), 1–18
Ren Jianye, Lei Chao. 2011. Tectonic stratigraphic framework of Yinggehai-Qiongdongnan Basins and its implication for tectonic province division in South China Sea. Chinese Journal of Geophysics (in Chinese), 54(12): 3303–3314
Rollins M S, Cohen A D, Durig J R. 1993. Effects of fires on the chemical and petrographic composition of peat in the Snuggedy Swamp, South Carolina. International Journal of Coal Geology, 22(2): 101–117, doi: 10.1016/0166-5162(93)90020-B
Shao Longyi, Dang Xingyu, Gao Xiangyu, et al. 2022a. Genetic mechanism of thick coal seams: astronomical-forcing superimposed multi-staged swamp model. Coal Science and Technology (in Chinese), 50(1): 186–195
Shao Lei, Meng Anhui, Li Qianyu, et al. 2017. Detrital zircon ages and elemental characteristics of the Eocene sequence in IODP Hole U1435A: Implications for rifting and environmental changes before the opening of the South China Sea. Marine Geology, 394: 39–51, doi: 10.1016/j.margeo.2017.08.002
Shao Longyi, Wen He, Gao Xiangyu, et al. 2022b. Identification of milankovitch cycles and calculation of net primary productivity of paleo-peatlands using geophysical logs of coal seams. Acta Geologica Sinica-English Edition, 96(6): 1830–1841, doi: 10.1111/1755-6724.14966
Shao Longyi, Xu Xiaotao, Wang Shuai, et al. 2021. Research progress of palaeogeography and palaeoenvironmental evolution of coal-bearing series in China. Journal of Palaeogeography (in Chinese), 23(1): 19–38
Shen Yulin, Qin Yong, Guo Yinghai, et al. 2016. Development characteristics of coal-measure source rocks divided on the basis of Milankovich coal accumulation cycle in Pinghu Formation, Xihu sag. Acta Petrolei Sinica (in Chinese), 37(6): 706–714
Tang Xiaoyin, Yang Shuchun, Hu Shengbiao. 2020. Provenance of the Paleogene sediments in the Pearl River Mouth Basin, northern South China Sea: Insights from zircon U-Pb and fission track double dating. Journal of Asian Earth Sciences, 200: 104494, doi: 10.1016/j.jseaes.2020.104494
Tardif D, Toumoulin A, Fluteau F, et al. 2021. Orbital variations as a major driver of climate and biome distribution during the greenhouse to icehouse transition. Science Advances, 7(43): eabh2819, doi: 10.1126/sciadv.abh2819
Thomson D J. 1982. Spectrum estimation and harmonic analysis. Proceedings of the IEEE, 70(9): 1055–1096, doi: 10.1109/PROC.1982.12433
Tyszka J. 2009. Foraminiferal response to seasonality modulated by orbital cycles in the Cretaceous mid-latitudes: The Albian record from the Lower Saxony Basin. Palaeogeography, Palaeoclimatology, Palaeoecology, 276(1–4): 148–159
Valero L, Garcés M, Cabrera L, et al. 2014. 20 Myr of eccentricity paced lacustrine cycles in the Cenozoic Ebro Basin. Earth & Planetary Science Letters, 408(1): 183–193
Valero L, Cabrera L, Sáez A, et al. 2016. Long-period astronomically-

forced terrestrial carbon sinks. Earth and Planetary Science Letters, 444: 131–138, doi: 10.1016/j.epsl.2016.03.038
Van Vugt N, de Bruijn H, van Kolfschoten M, et al. 2000. Magneto- and cyclostratigraphy and mammal-fauna's of the Pleistocene lacustrine Megalopolis Basin, Peloponnesos, Greece. Geologica Ultraiectina, 189: 69–92
Van Vugt N, Langereis C G, Hilgen F J. 2001. Orbital forcing in Pliocene-Pleistocene Mediterranean lacustrine deposits: dominant expression of eccentricity versus precession. Palaeogeography, Palaeoclimatology, Palaeoecology, 172(3–4): 193–205
Vázquez A, Utrilla R, Zamarreño I, et al. 2000. Precession-related sapropelites of the Messinian Sorbas Basin (South Spain): paleoenvironmental significance. Palaeogeography, Palaeoclimatology, Palaeoecology, 158(3–4): 353–370
Wang Pengcheng, Li Sanzhong, Guo Lingli, et al. 2017. Opening of the South China Sea (SCS): ajoint effect of dextral strike-slip pull-apart and proto-SCS slab pull. Earth Science Frontiers (in Chinese), 24(4): 294–319
Wang Dongdong, Li Zengxue, Zhang Gongcheng, et al. 2011. Base level cycles division and switch mechanism of oligocene epoch Yacheng formation in Qiongdongnan basin. Journal of China University of Mining & Technology (in Chinese), 40(4): 576–583
Wang Dongdong, Zhang Gongcheng, Li Zengxue, et al. 2021. The development characteristics and distribution predictions of the Paleogene coal-measure source rock in the Qiongdongnan Basin, Northern South China Sea. Acta Geologica Sinica (English Edition), 95(1): 105–120, doi: 10.1111/1755-6724.14625
Wei Xiaosong, Yan Detian, Luo Pan, et al. 2020. Astronomically forced climate cooling across the Eocene–Oligocene transition in the Pearl River Mouth Basin, northern South China Sea. Palaeogeography, Palaeoclimatology, Palaeoecology, 558: 109945
Weedon G P. 2003. Time-Series Analysis and Cyclostratigraphy: Constructing time series in cyclostratigraphy. Cauces Cuadernos Del Consejo Económico Y Social, 134(s1-2): 77–78.
Wu Guoxuan, Qin Jungan, Mao Shaozhi. 2003. Palynological records of the Xiocene series of the deep sea facies in the South China Sea. Chinese Science Bulletin (in Chinese), 48(17): 1868–1871, doi: 10.1360/csb2003-48-17-1868
Wu Yuxiang, Shu Yu, Ding Lin, et al. 2021. Prediction of high quality source rocks based on sequence stratigraphic framework of Wenchang formation, Panyu 4 depression, the Pearl River Mouth Basin. Marine Geology Frontiers (in Chinese), 37(3): 41–49
Wu Huaichun, Zhang Shihong, Feng Qinglai, et al. 2011. Theoretical basis, research advancement and prospects of cyclostratigraphy. Earth Science (in Chinese), 36(3): 409–428
Wu Huaichun, Zhang Shihong, Jiang Ganqing, et al. 2013. Astrochronology of the Early Turonian–Early Campanian terrestrial succession in the Songliao Basin, northeastern China and its implication for long-period behavior of the Solar System. Palaeogeography, Palaeoclimatology, Palaeoecology, 385: 55–70
Xu Ke, Kemp D B, Ren Jianye, et al. 2023. Astronomically forced climate variability across the Eocene–Oligocene transition from a low latitude terrestrial record (Lühe Basin, South China). GSA Bulletin, 135(9-10): 2678–2690
Xia Wenyue. 2022. Cyclostratigraphy on the Eocene Wenchang Formation in the Pearl River Mouth Basin (in Chinese)[dissertation]. Beijing: China University of Geosciences.
Yin Lusheng. 2022. Coal-forming Sedimentary Environment and Coal Accumulation Law of the Paleogene Enping Formation in the Zhu Ⅰ Depression (in Chinese)[dissertation]. Shandong University of Science and Technology.
Zhang Gongcheng. 2010. Tectonic evolution of deepwater area of northern continental margin in South China Sea. Acta Petrolei Sinica (in Chinese), 31(4): 528–533,541
Zhang Gongcheng, Chen Ying, Li Zengxue, et al. 2022. Theory on genesis of coaliferous petroleum in the China Sea. Oil & Gas Geology (in Chinese), 43(3): 553–565
Zhang Gongcheng, Jia Qingjun, Wang Wanyin, et al. 2018. On tectonic framework and evolution of the South China Sea. Chinese Journal of Geophysics (in Chinese), 61(10): 4194–4215
Zhang Gongcheng, Li Zengxue, Wang Dongdong, et al. 2020c. Characteristics of coal geology in South China Sea. Journal of China Coal Society (in Chinese), 45(11): 3864–3878
Zhang Gongcheng, Mi Lijun, Wu Shiguo, et al. 2007. Deepwater area-the new prospecting targets of northern continental margin of South China Sea. Acta Petrolei Sinica (in Chinese), 28(2): 15–21
Zhang Gongcheng, Qu Hongjun, Liu Shixiang, et al. 2015b. Tectonic cycle of marginal sea controlled the hydrocarbon accumulation in deep-water areas of South China Sea. Acta Petrolei Sinica (in Chinese), 36(5): 533–545
Zhang Chunliang, Shen Yulin, Qin Yong, et al. 2016a. Development regularities of the coal-measure source rock in Ya-3 member of Yacheng formation, well Y1, in Yanan depression within Qiongdongnan Basin. Acta Sedimentologica Sinica (in Chinese), 34(5): 1003–1010
Zhang Lili, Shu Liangfeng, Feng Xuan, et al. 2020a. Further discussion on the age assignment of Enping Formation in the Pearl River Mouth basin. China Offshore Oil and Gas (in Chinese), 32(5): 9–18
Zhang Zhihui, Wang Chengshan, Lü Dawei, et al. 2020b. Precession-scale climate forcing of peatland wildfires during the early middle Jurassic greenhouse period. Global and Planetary Change, 184: 103051, doi: 10.1016/j.gloplacha.2019.103051
Zhang Gongcheng, Wang Qi, Miao Shunde, et al. 2014b. The duality distribution pattern of marine-continental transitional hydrocarbon source rocks: A case study from Baiyun Sag in Pearl River Mouth Basin, China offshore. Natural Gas Geoscience (in Chinese), 25(9): 1299–1308
Zhang Gongcheng, Wang Pujun, Wu Jingfu, et al. 2015a. Tectonic cycle of marginal oceanic basin: a new evolution model of the South China Sea. Earth Science Frontiers (in Chinese), 22(3): 27–37
Zhang Gongcheng, Xie Xiaojun, Wang Wanyin, et al. 2013. Tectonic types of petroliferous basins and its exploration potential in the South China Sea. Acta Petrolei Sinica (in Chinese), 34(4): 611–627
Zhang Gongcheng, Yang Haizhang, Chen Ying, et al. 2014a. The Baiyun Sag: a giant rich gas-generation sag in the deepwater area of the Pearl River Mouth Basin. Natural Gas Industry (in Chinese), 34(11): 11–25
Zhang Gongcheng, Zeng Qingbo, Su Long, et al. 2016b. Accumulation mechanism of LS17–2 deep water giant gas field in Qiongdongnan Basin. Acta Petrolei Sinica (in Chinese), 37(S1): 34–46
Zhang Gongcheng, Zhu Weilin, Mi Lijun, et al. 2010. The theory of hydrocarbon Genernation controlled by source rock and heat from circle distribution of outside-oil fields and inside-gas fields in South China Sea. Acta Sedimentologica Sinica (in Chinese), 28(5): 987–1005
Zhao Ke, Du Xuebin, Jia Jixin, et al. 2021. Effects of sea-level variation and sedimentary noise variation on the development of biogenic reefs since the Pliocene among the Xisha Islands, South China Sea. Geological Society of America Bulletin, 134(7-8): 1781–1792
Zhao Ke, Du Xuebin, Jia Jixin, et al. 2022. Orbitally controls of climate recorded in a series of thin-multiple-layers coal seams in marine–continent transition environment during late Eocene. Palaeogeography, Palaeoclimatology, Palaeoecology, 606: 111233
Zhou Fengjuan, Ding Lin, Ma Yongkun, et al. 2020. Detrital zircon U-Pb age characteristics of Wenchang Formation in Lufeng 13 eastern sag and its significance for provenance tracing. China Offshore Oil and Gas (in Chinese), 32(4): 46–55
Zhu Mingyu, Shao Longyi, Sun Bin, et al. 2022. Sequence paleogeography and coal accumulation model in the fluvio-lacustrine rift basin: The Lower Cretaceous of the Huhehu Sag of Hailar Basin, Inner Mongolia (NE China). Marine and Petroleum Geology, 145: 105879, doi: 10.1016/j.marpetgeo.2022.105879